

# A non zero $\theta_{13}$ from a minimal and predictive neutrino mass matrix

Sagar Tirtha Goswami,<sup>1,\*</sup> Pralay Chakraborty,<sup>1,†</sup> and Subhankar Roy<sup>1,‡</sup>

<sup>1</sup>*Department of Physics, Gauhati University, Assam-781014, India*

(Dated: June 25, 2025)

We propose a new, minimal Majorana neutrino mass matrix texture and study its predictions within a partial tri-bimaximal (TBM) mixing scheme, where  $\sin \theta_{12} = 1/\sqrt{3}$  and  $\sin \theta_{23} = 1/\sqrt{2}$ , with  $\theta_{13}$  and  $\delta$  treated as free parameters. The texture forbids  $\theta_{13} = 0$  and does not correspond to a  $\mu$ - $\tau$  symmetric structure. We find that the predictions show distinct behavior depending on the sign of a single real texture parameter. The texture is realized through a hybrid framework of one Type-I seesaw and two Type-II seesaw mechanisms under an extended symmetry group,  $SU(2)_L \otimes U(1)_Y \otimes A_4 \otimes Z_{10} \otimes Z_7$  with properly chosen model parameters. The texture is seen to favor the normal hierarchy for neutrino masses.

## I. INTRODUCTION

In the realm of particle physics, neutrino ( $\nu$ ) is the most evasive particle. The standard model (SM), which is quite successful in describing the properties of other particles, has proved to be inadequate in the neutrino sector. In particular, the SM is silent on two key issues: the origin of tiny but non-zero masses of neutrinos, confirmed by various neutrino oscillation experiments [1–10], and the significant mixing among different flavours of neutrinos [11, 12]. The quest to find answers to these unresolved questions among many others has led us beyond the SM (BSM), which is an arena of various models and conjectures. These models try to predict some observational parameters related to neutrinos, such as the mass squared differences ( $\Delta m_{21}^2$  and  $\Delta m_{31}^2$ ), three mixing angles ( $\theta_{12}, \theta_{23}$  and  $\theta_{13}$ ), one Dirac CP-violating phase ( $\delta$ ) and two Majorana CP-violating phases ( $\alpha$  and  $\beta$ ). So far, the experiments have determined the mass squared differences and the mixing angles with great precision [12]. But the octant of  $\theta_{23}$ , and precise range of  $\delta$  are still undetermined. In addition, the individual mass eigenvalues ( $m_1, m_2$  and  $m_3$ ) and Majorana phases ( $\alpha, \beta$ ) are not witnessed by oscillation experiments.

The information about all the parameters mentioned above is contained in the Majorana neutrino mass matrix ( $M_\nu$ ). Although a complete quantitative determination of the observable parameters remains unavailable, even the limited information already provides valuable insights into the underlying symmetries governing neutrino mass and mixing patterns. Based on this knowledge, the theorists, in general, try to obtain the  $M_\nu$  from first principle, which predict not only the observable parameters already determined, but also the ones yet to be measured. However, as we wait to see experimental verification of these predictions, certainly avenues are open for the proposition of a new  $M_\nu$ .

As a common practice, some phenomenological ideas such as  $\mu - \tau$  symmetry [13–15], texture zeroes [16], hybrid textures [17, 18] etc., are assigned to  $M_\nu$  to expect certain results of the observational parameters. These results, which can be called mixing schemes, basically involve the mixing angles and the Dirac CP phase. Over the time, different mixing schemes have been postulated, which are related to specific phenomenological forms of  $M_\nu$ . For example, if we talk about  $\mu - \tau$  symmetry, we see that the mixing scheme predicted by such a texture always has  $\theta_{23} = 45^\circ$  and  $\theta_{13} = 0$ , while  $\theta_{12}$  remains free and is related to texture parameters. A careful calibration of the texture parameters can make  $\sin \theta_{12} = 1/\sqrt{3}$  and this particular mixing scheme is known as TBM mixing [19].

However, it is important to note that the value of  $\theta_{13}$  is found to be non-zero [7], which is a contradicts the original TBM scheme and is inconsistent with the prediction of a  $\mu - \tau$  symmetric texture. Interestingly the other two angles,  $\theta_{12}$  and  $\theta_{23}$ , still lie within the  $3\sigma$  range of present experimental data [11, 12]. This renders the TBM scheme only partially viable, while ruling out the strict realization of  $\mu - \tau$  symmetry.

This partial validity of TBM scheme opens two interesting possibilities. One is based on a top down approach in which new textures are put forward from first principle to predict a non zero  $\theta_{13}$ , while resembling the TBM scheme in other aspects. A common way in this regard is the addition of corrections to a  $\mu - \tau$  symmetric texture through various means [15, 20–28]. The other one is based on a bottom up approach in which one can choose a valid partial TBM scheme and apply it to a texture to study its phenomenology.

In this work, we take a bottom up approach in which we adopt a partial TBM scheme. But rather than fixing  $\theta_{13}$  with a single value, we keep it as a free parameter. We also posit a new minimal Majorana mass matrix texture and

\* sagartirtha@gauhati.ac.in

† pralay@gauhati.ac.in

‡ subhankar@gauhati.ac.in

try to see its various predictions under the chosen mixing scheme. Then we relax the the values of  $\theta_{12}$  and  $\theta_{23}$  to see how its predictions compare to the previous ones.

The plan of the paper is as follows: In Section II, we discuss the formalism of our work, while in Section III, we discuss the results of our texture under various conditions. Section IV contains some applications of our texture, while in Section V, a symmetry perspective of our proposed texture is discussed. Finally we give a summary of our work in Section VI.

## II. FORMALISM

We begin by outlining the theoretical framework used in this work. This includes the structure of the proposed Majorana mass matrix texture and the parametrization of the leptonic mixing matrix under the partial TBM scheme ( $\sin \theta_{12} = 1/\sqrt{3}$ ,  $\sin \theta_{23} = 1/\sqrt{2}$ , while  $\theta_{13}$  and  $\delta$  being free parameters), as discussed in Section I.

The Majorana mass matrix texture proposed in this work is given by,

$$M_\nu = \begin{bmatrix} a + \frac{9}{5}h & a + b & -a + b \\ a + b & a + g + h & -a + g \\ -a + b & -a + g & a + g - h \end{bmatrix}, \quad (1)$$

where the four parameters,  $a$ ,  $b$ ,  $g$ , and  $h$  are complex in general.

To obtain the information of the physical parameters, we need to diagonalize  $M_\nu$  with Potecorvo-Maki-Nakagawa-Sakata (PMNS) matrix,  $U$  [29], as shown below,

$$M_\nu^{diag} = U^T M_\nu U,$$

where

$$U = \begin{bmatrix} e^{i\phi_1} & 0 & 0 \\ 0 & e^{i\phi_2} & 0 \\ 0 & 0 & e^{i\phi_3} \end{bmatrix} \times \begin{bmatrix} 1 & 0 & 0 \\ 0 & c_{23} & s_{23} \\ 0 & -s_{23} & c_{23} \end{bmatrix} \times \begin{bmatrix} c_{13} & 0 & -s_{13} e^{-i\delta} \\ 0 & 1 & 0 \\ s_{13} e^{i\delta} & 0 & c_{13} \end{bmatrix} \times \begin{bmatrix} c_{12} & s_{12} & 0 \\ -s_{12} & c_{12} & 0 \\ 0 & 0 & 1 \end{bmatrix}, \quad (2)$$

with  $s_{ij} = \sin \theta_{ij}$  and  $c_{ij} = \cos \theta_{ij}$ . It is to be mentioned that the unphysical phases  $\phi_1$ ,  $\phi_2$  and  $\phi_3$  can be absorbed by the redefinition of the charged lepton fields in terms of these phases. In general, the Majorana phases  $\alpha$  and  $\beta$  are embedded into  $U$ . On the other hand, these phases can also be placed inside the diagonal neutrino mass matrix. The present work adopts the latter approach as shown below,

$$M_\nu^{diag} = \begin{bmatrix} m_1 e^{-2i\alpha} & 0 & 0 \\ 0 & m_2 e^{-2i\beta} & 0 \\ 0 & 0 & m_3 \end{bmatrix}.$$

The advantage of the above mentioned parametrization of  $M_\nu^{diag}$  is that the Majorana phases  $\alpha$  and  $\beta$  can be directly obtained from the following relations,

$$\begin{aligned} \alpha &= -\frac{1}{2} \text{Arg} [M_{\nu_{11}}^{diag}], \\ \beta &= -\frac{1}{2} \text{Arg} [M_{\nu_{22}}^{diag}]. \end{aligned} \quad (3)$$

The present analysis involves four complex texture parameters and nine observational parameters. We have three complex diagonalizing conditions, viz.,  $M_{\nu_{12}}^{diag} = 0$ ,  $M_{\nu_{13}}^{diag} = 0$ ,  $M_{\nu_{23}}^{diag} = 0$ , appearing as transcendental equations. Additionally, the chosen parametrization ensures that  $M_{\nu_{33}}^{diag}$  is real. Therefore, if we exploit these conditions, some of the free parameters can be reduced.

Now, if we apply our chosen partial TBM scheme to  $U$  (Eq. 2), we find the following three relations from the diagonalization conditions,

$$a = \frac{h}{\sqrt{2}} \cot \theta_{13} e^{i\delta}, \quad (4)$$

$$b = \frac{h}{2} \cot \theta_{13} \left[ -\frac{9\sqrt{2}}{5} e^{-i\delta} - \tan \frac{\theta_{13}}{2} \right], \quad (5)$$

$$g = \frac{h e^{-2i\delta}}{8} \left[ \frac{36 \cot^2 \theta_{13}}{5} + \frac{\sqrt{2} e^{i\delta} \csc \theta_{13}}{1 + \cos \theta_{13}} (1 + 2 \cos \theta_{13} + 3 \cos 2\theta_{13}) \right]. \quad (6)$$

Further, on applying the constraint that  $M_{\nu 33}^{diag}$  is real, we reduce another parameter,  $\text{Im}[h]$  as follows,

$$\text{Im}[h] = \frac{\text{Re}[h] \sin \delta \left[ 72 \cos \delta \cos \left( \frac{\theta_{13}}{2} \right) + 5\sqrt{2} \left( \sin \left( \frac{\theta_{13}}{2} \right) + \sin \left( \frac{5\theta_{13}}{2} \right) \right) \right]}{36 \cos(2\delta) \cos \left( \frac{\theta_{13}}{2} \right) + 5\sqrt{2} \cos \delta \left( \sin \left( \frac{\theta_{13}}{2} \right) + \sin \left( \frac{5\theta_{13}}{2} \right) \right)}. \quad (7)$$

So, from Eqs. (4)-(7), we can say that there are three free parameters, viz.,  $\text{Re}[h]$ ,  $\theta_{13}$  and  $\delta$ , that determine the predictions of the texture (Eq. 1). Again, from Eq. (4), we can relate  $\theta_{13}$  and  $\delta$  to texture parameters via two simple relations as shown in the following,

$$\sin^2 \theta_{13} = \frac{1}{1 + 2 \left| \frac{a}{h} \right|^2}, \quad \delta = \arg \left[ \frac{a}{h} \right].$$

From Eq. (4), it is easy to see that if  $\theta_{13} = 0$ , the three texture parameters,  $a$ ,  $b$ , and  $g$  become undefined. Hence, our proposed texture (Eq. (1)) strictly forbids a vanishing  $\theta_{13}$  under the chosen mixing scheme. Likewise, we can not have  $h = 0$ , as it would collapse the whole texture. Hence, the proposed texture is not simply a  $\mu - \tau$  deviated texture.

In addition to the texture relations (Eqs. (4)-(7)), we can express three  $\nu$  mass eigenvalues and the two Majorana phases in terms of  $\text{Re}[h]$ ,  $\theta_{13}$  and  $\delta$ . It is notable that, under the chosen partial TBM scheme, the two Majorana phases are equal. The expressions for the mass eigenvalues and phases are given as follows,

$$\begin{aligned} \alpha &= \beta = \frac{1}{2} \tan^{-1} \left[ \frac{18\sqrt{2} \cos \left( \frac{\theta_{13}}{2} \right) \sin 3\delta + 5 \sin 2\delta \left( \sin \left( \frac{\theta_{13}}{2} \right) + \sin \left( \frac{5\theta_{13}}{2} \right) \right)}{18\sqrt{2} \cos \left( \frac{\theta_{13}}{2} \right) \cos 3\delta + 5 \cos 2\delta \left( \sin \left( \frac{\theta_{13}}{2} \right) + \sin \left( \frac{5\theta_{13}}{2} \right) \right)} \right], \\ m_1 &= \frac{1}{\left[ 36 \cos 2\delta \cos \left( \frac{\theta_{13}}{2} \right) + 5\sqrt{2} \cos \delta \left( \sin \left( \frac{\theta_{13}}{2} \right) + \sin \left( \frac{5\theta_{13}}{2} \right) \right) \right]} \left[ (\text{Re}[h])^2 \sin^2 \theta_{13} \sec^4 \left( \frac{\theta_{13}}{2} \right) (349 + 90\sqrt{2} \right. \\ &\quad \left. \cos \delta (\sin \theta_{13} + \sin 2\theta_{13} + \sin 3\theta_{13}) + \frac{623 \cos \theta_{13}}{2} + 25 \cos 2\theta_{13} - 25 \cos 3\theta_{13} - \frac{25}{2} \cos 5\theta_{13}) \right]^{1/2}, \\ m_2 &= \frac{1}{\sqrt{2} [20\sqrt{2} \cos \delta \cos^2 \left( \frac{\theta_{13}}{2} \right) (1 + \cos \theta_{13} + \cos 2\theta_{13}) \sin^4 \left( \frac{\theta_{13}}{2} \right) + 9 \cos 2\delta \sin^3 \theta_{13}] } \left[ (698 + 623 \cos \theta_{13} \right. \\ &\quad \left. + 50 \cos 2\theta_{13} - 50 \cos 3\theta_{13} - 25 \cos 5\theta_{13} + 180\sqrt{2} \cos \delta (\sin \theta_{13} + \sin 2\theta_{13} + \sin 3\theta_{13})) (\text{Re}[h])^2 \cos^2 \right. \\ &\quad \left. \left( \frac{\theta_{13}}{2} \right) \sin^4 \left( \frac{\theta_{13}}{2} \right) (1 + 2 \cos \theta_{13})^2 \right]^{1/2}, \\ m_3 &= \frac{1}{20 [5\sqrt{2} \cos \delta (1 + \cos \theta_{13} + \cos 2\theta_{13}) + 180 \cos 2\delta \cot \left( \frac{\theta_{13}}{2} \right)] } \left[ 360\sqrt{2} \cos \delta (1 + \cos \theta_{13} + \cos 2\theta_{13}) \right. \\ &\quad \left. + 623 \cot \theta_{13} + (698 + 50 \cos 2\theta_{13} - 50 \cos 3\theta_{13} - 25 \cos 5\theta_{13}) \csc \theta_{13} \right] \text{Re}[h] \csc^2 \theta_{13}. \end{aligned} \quad (8)$$

In the next section, we will try to visualize the numerical ranges of the physical parameters.

### III. NUMERICAL ANALYSIS

In this section, we will try to observe the patterns of the physical parameters (Eq. (8)), and extract their numerical bounds. For that, we take  $3\sigma$  ranges [11] of two of the input parameters,  $\theta_{13}$  and  $\delta$ , while varying  $\text{Re}[h]$  randomly in the interval  $[-1, 1]$ . Interestingly, two distinct scenarios for the features of the observable parameters emerge, depending on the sign of  $\text{Re}[h]$ . We categorise the results into two cases as shown below,

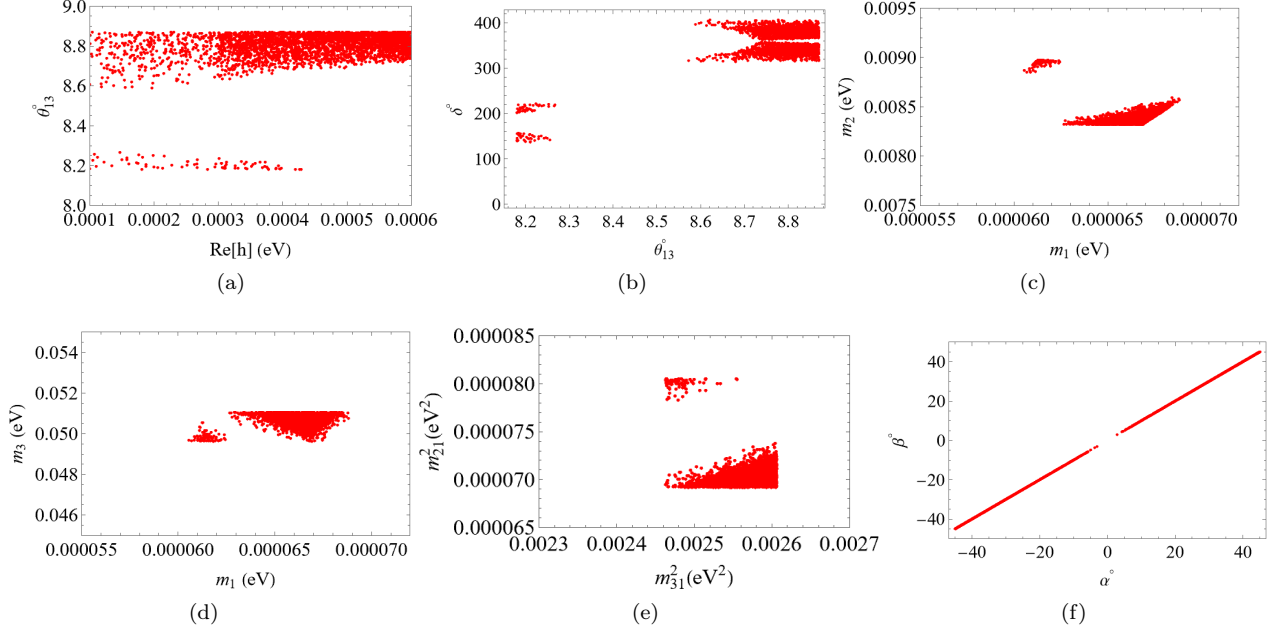


FIG. 1. The correlation plots between (a)  $\theta_{13}$  vs  $\text{Re}[h]$ , (b)  $\delta$  vs  $\theta_{13}$ , (c)  $m_2$  vs  $m_1$ , (d)  $m_3$  vs  $m_1$ , (e)  $\Delta m_{21}^2$  vs  $\Delta m_{31}^2$  and (f)  $\beta$  vs  $\alpha$  for  $\text{Re}[h] > 0$  under the partial TBM scheme.

### Case 1

First, we discuss the case,  $\text{Re}[h] > 0$  and find that many observable show peculiarities within their ranges. We summarise the main results as follows,

- We see that the angle,  $\theta_{13}$  shows a gap within its  $3\sigma$  range [11], as can be seen from Figs. 1(a) and 1(b). This gap is approximately from  $8.26^\circ$  to  $8.58^\circ$ .
- We can also see the same in the  $3\sigma$  bounds [11] of  $\delta$ . In fact, in this case, there are two such gaps, from  $157^\circ$  to  $194^\circ$  and  $219^\circ$  to  $316^\circ$ , as seen from Fig. 1(b).
- We see bounds on the values of  $m_1, m_2$  and  $m_3$  as  $6.07 \times 10^{-5} \text{ eV} < m_1 < 6.92 \times 10^{-5} \text{ eV}$ ,  $0.00827 \text{ eV} < m_2 < 0.00898 \text{ eV}$  and  $0.049 \text{ eV} < m_3 < 0.051 \text{ eV}$  approximately (see Figs. 1(c) and 1(d)). Interestingly,  $m_1$  and  $m_2$  show some gaps in their values. For  $m_1$ , the forbidden interval is  $(6.28 \times 10^{-5} \text{ eV} - 6.32 \times 10^{-5} \text{ eV})$ , while for  $m_2$ , it is  $(0.00863 \text{ eV} - 0.00886 \text{ eV})$ .
- We can see a similar pattern in the values of  $\Delta m_{21}^2$ , with the forbidden region lying from  $7.45 \times 10^{-5} \text{ eV}^2 - 7.83 \times 10^{-5} \text{ eV}^2$ , as seen from Fig. 1(e).
- Regarding the two Majorana phases, we observe that they are equal and span a range from about  $-45^\circ$  to  $45^\circ$ . Further, they too exhibit an identical gap in their allowed ranges, approximately between  $0^\circ$  and  $5^\circ$  (see Fig. 1(f)).

### Case 2

We now move to discuss the second case, viz.,  $\text{Re}[h] < 0$  and the main observations are presented here,

- From Fig. 2, we observe that, unlike the previous case, the parameters here do not exhibit gaps in their allowed ranges, except for  $\delta$ . The two forbidden regions for  $\delta$  lie approximately from  $122^\circ$  to  $233^\circ$  and  $300^\circ$  to  $420^\circ$  within the  $3\sigma$  bounds [11].
- The values of  $m_1, m_2$  and  $m_3$  are constrained to the approximate ranges  $(5.74 \times 10^{-5} \text{ eV} - 7.26 \times 10^{-5} \text{ eV})$ ,  $(0.00830 \text{ eV} - 0.00894 \text{ eV})$  and  $(0.0495 \text{ eV} - 0.0510 \text{ eV})$  respectively, but without any forbidden regions, as observed in Figs. 2(c) and 2(d).
- Like in the previous case, the two Majorana phases are equal and have the same ranges but without any forbidden gaps in their ranges (see Fig. 2(f)).

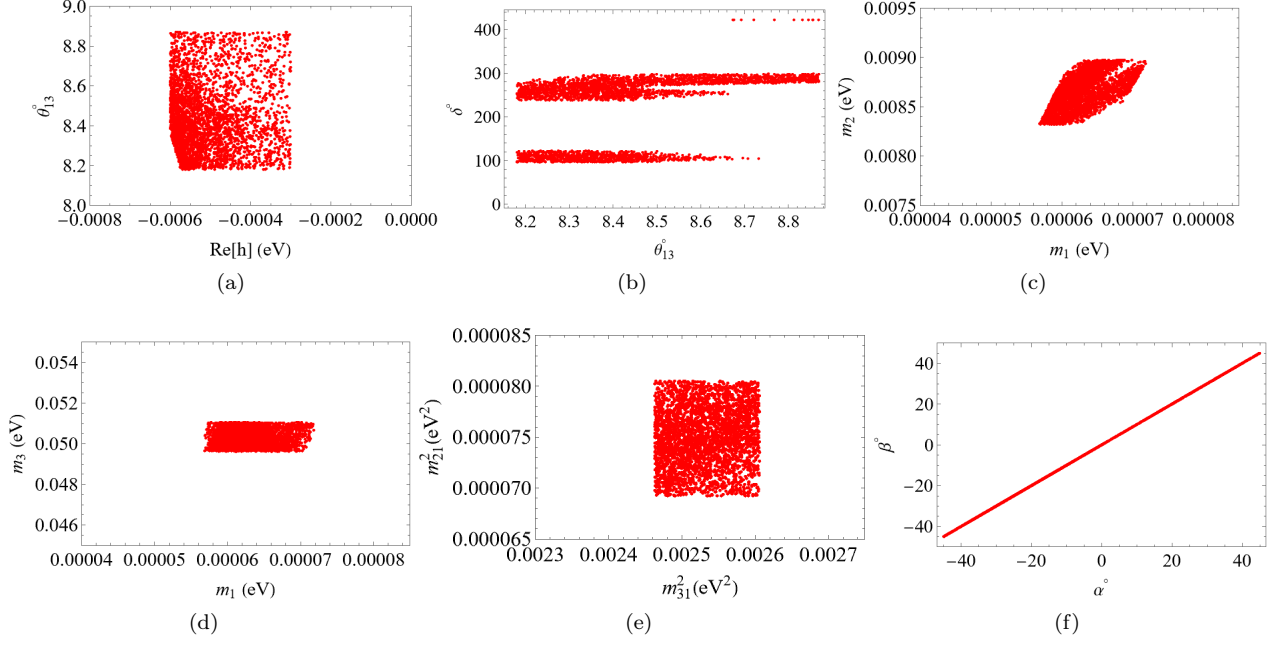


FIG. 2. The correlation plots between (a)  $\theta_{13}$  vs  $\text{Re}[h]$ , (b)  $\delta$  vs  $\theta_{13}$ , (c)  $m_2$  vs  $m_1$ , (d)  $m_3$  vs  $m_1$ , (e)  $\Delta m_{21}^2$  vs  $\Delta m_{31}^2$  and (f)  $\beta$  vs  $\alpha$  for  $\text{Re}[h] < 0$  under the partial TBM scheme.

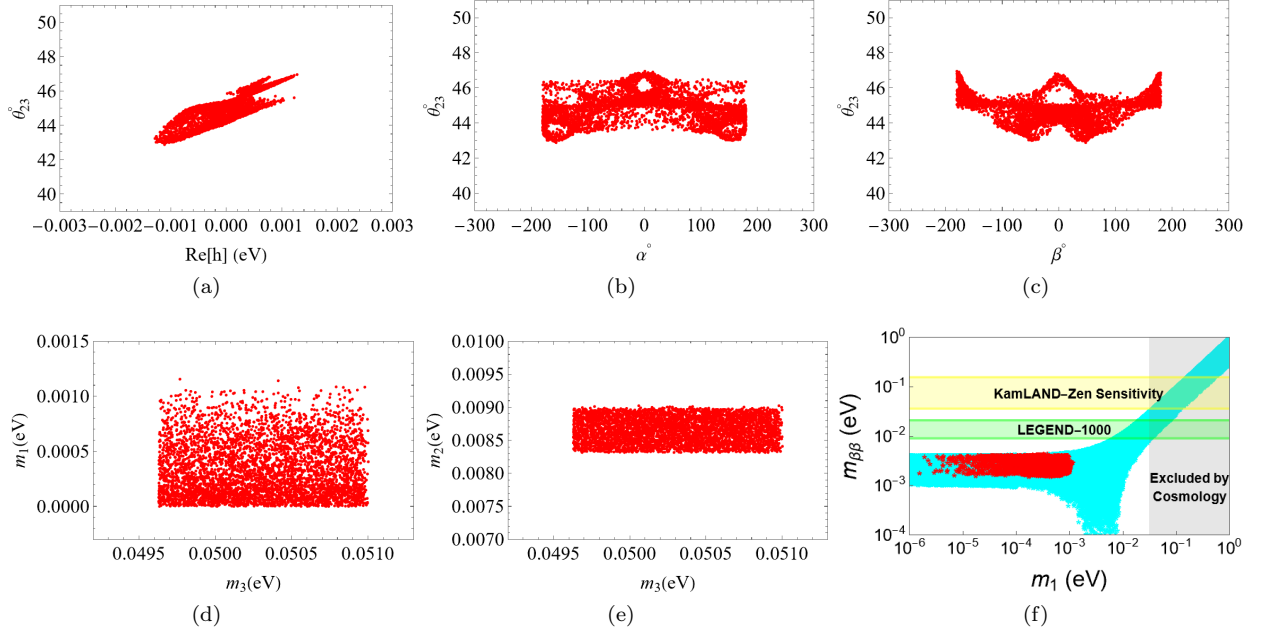


FIG. 3. The correlation plots between (a)  $\theta_{23}$  vs  $\text{Re}[h]$ , (b)  $\theta_{23}$  vs  $\alpha$ , (c)  $\theta_{23}$  vs  $\beta$ , (d)  $m_1$  vs  $m_3$ , (e)  $m_2$  vs  $m_3$  and (f) the predicted values of  $m_{\beta\beta}$  of our texture under a fully randomized  $U$ .

Having discussed the results under the chosen partial TBM scheme with fixed values of  $\theta_{12}$  and  $\theta_{23}$ , we now extend our analysis by considering a more general scenario, i.e., allowing these two parameters to vary within their respective  $3\sigma$  bounds [11]. As a result, the predictions for the observable parameters are modified. We summarize the findings as follows,

- We see from Figs. 3(a), 3(b) and 3(c) that the values of  $\theta_{23}$  are constrained to a narrow range of  $(43^\circ - 47^\circ)$  within its  $3\sigma$  range [11].

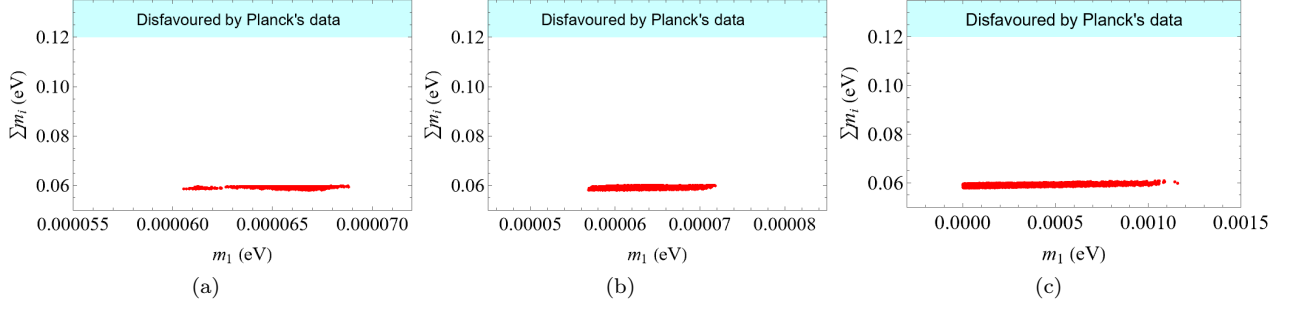


FIG. 4. The correlation plots between (a)  $\Sigma m_i$  vs  $m_1$  for  $\text{Re}[h] > 0$  under the partial TBM scheme, (b)  $\Sigma m_i$  vs  $m_1$  for  $\text{Re}[h] < 0$  under the partial TBM scheme, (c)  $\Sigma m_i$  vs  $m_1$  under a fully randomized  $U$ .

- Unlike in the fixed mixing scheme, the two Majorana phases are not equal and they both occupy a wider interval  $[-175^\circ, 175^\circ]$  approximately (see Figs. 3(b) and 3(c)).
- The value of  $m_1$  is constrained to a wider range of approximately  $(10^{-6} \text{ eV} - 0.0015 \text{ eV})$  compared to the previous cases. The values of  $m_2$  and  $m_3$  are constrained to the ranges  $(0.0083 \text{ eV} - 0.0089 \text{ eV})$  and  $(0.04962 \text{ eV} - 0.05102 \text{ eV})$  approximately (see Figs. 3(d) and 3(e)).
- For other observable parameters such as  $\theta_{13}$ ,  $\theta_{12}$  and  $\delta$ , no constraints or patterns are observed in their  $3\sigma$  ranges [11].

We observe that, under a completely randomized  $U$ , the predictions of our proposed texture deviate from those obtained under the partial TBM mixing scheme. Two notable features in this case are the absence of discontinuities in the allowed ranges of the observable parameters and the inequality between  $\alpha$  and  $\beta$ . Moreover, the sign of  $\text{Re}[h]$  does not affect the predictions for the randomized  $U$  case unlike the partial TBM case. Nevertheless, both scenarios exclusively favor the NH for neutrino masses. In addition, the sum of the three mass eigenvalues for all the three cases, as shown in Fig. 4(a)-4(c), lie well below the cosmological upper bounds [30].

In the next section, we shall attempt to examine the viability of the proposed texture further, by studying its implications for other phenomenologically relevant observables.

#### IV. APPLICATION

We now explore two key phenomenological applications of the proposed texture, focusing on its predictions for effective neutrino mass and the CP asymmetry parameter, under a fully randomized  $U$ .

##### A. Effective Majorana Neutrino Mass

Neutrinoless double beta decay ( $0\nu\beta\beta$ ) [31] is a lepton number violating process, and its observation would confirm the Majorana nature of neutrinos. The decay rate  $\Gamma$  is determined by the phase space factor  $G_{0\nu}$ , the nuclear matrix element  $M_{0\nu}$ , and the effective Majorana mass ( $m_{\beta\beta}$ ), following the relation:

$$\Gamma \sim G_{0\nu} \cdot M_{0\nu} \cdot m_{\beta\beta}^2.$$

The  $m_{\beta\beta}$  is an experimentally accessible parameter and is given by:

$$m_{\beta\beta} = \left| \sum_{k=1}^3 U_{1k}^2 m_k \right|,$$

where  $m_1, m_2, m_3$  are the neutrino mass eigenvalues, and  $U_{11}, U_{12}, U_{13}$  are elements of  $U$ . The Majorana phases are embedded with  $m_1$  and  $m_2$ , based on our chosen parametrization (Eq. (3)).

Several experiments have placed upper bounds on  $m_{\beta\beta}$ : SuperNEMO ( $\text{Se}^{82}$ ) at  $(67 - 131) \text{ meV}$ , GERDA ( $\text{Ge}^{76}$ ) at  $(104 - 228) \text{ meV}$ , EXO-200 ( $\text{Xe}^{136}$ ) at  $(111 - 477) \text{ meV}$ , CUORE ( $\text{Te}^{130}$ ) at  $(75 - 350) \text{ meV}$ , KamLAND-Zen ( $\text{Xe}^{136}$ ) at  $(61 - 165) \text{ meV}$  and LEGEND-1000 ( $\text{Ge}^{76}$ ) at  $(9.4 - 21.4) \text{ meV}$  [32–38].

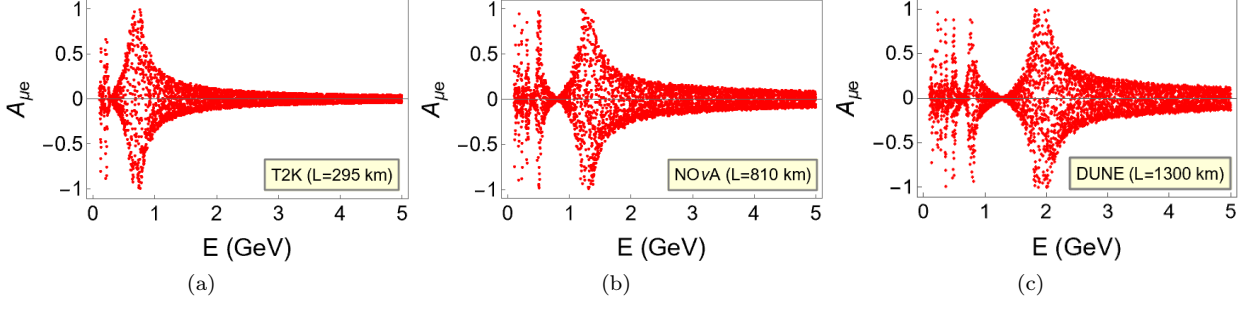


FIG. 5. The correlation plots between (a)  $A_{\mu e}$  vs  $E$  for T2K ( $L = 295$  km), (b)  $A_{\mu e}$  vs  $E$  for NO $\nu$ A ( $L = 810$  km), (c)  $A_{\mu e}$  vs  $E$  for DUNE ( $L = 1300$  km) for the inverted ordering of neutrino masses.

In light of these experimental bounds, we examine the prediction for  $m_{\beta\beta}$  from the proposed texture, as illustrated in Fig. 3(f). The predicted range,  $(1.55 - 4.39)$  meV lies below the projected sensitivities of many current and upcoming experiments. This suggests that the prediction could become testable with the advent of more sensitive and sophisticated future experiments.

### B. CP Asymmetry Parameter

Leptonic Dirac CP violation, characterized by the phase  $\delta$ , can manifest in neutrino oscillations through the CP asymmetry parameter  $A_{\mu e}$  [39], defined as:

$$A_{\mu e} = \frac{P(\nu_\mu \rightarrow \nu_e) - P(\bar{\nu}_\mu \rightarrow \bar{\nu}_e)}{P(\nu_\mu \rightarrow \nu_e) + P(\bar{\nu}_\mu \rightarrow \bar{\nu}_e)}.$$

The transition probability  $P(\nu_\mu \rightarrow \nu_e)$  can be expressed in terms of physical parameters as follows:

$$P(\nu_\mu \rightarrow \nu_e) = P_{\text{atm}} + P_{\text{sol}} + 2\sqrt{P_{\text{atm}}} \sqrt{P_{\text{sol}}} \cos(\Delta_{ij} + \delta),$$

where  $\Delta_{ij} = \Delta m_{ij}^2 \cdot \frac{L}{4E}$ , with  $E$  denoting the neutrino beam energy and  $L$  the baseline length. The quantities  $P_{\text{atm}}$  and  $P_{\text{sol}}$  are given by:

$$P_{\text{atm}} = \sin \theta_{23} \sin 2\theta_{13} \cdot \frac{\sin(\Delta_{31} - aL)}{(\Delta_{31} - aL)} \cdot \Delta_{31}, \quad P_{\text{sol}} = \cos \theta_{23} \sin 2\theta_{12} \cdot \frac{\sin(aL)}{aL} \cdot \Delta_{21}.$$

The parameter  $a = \frac{G_F N_e}{\sqrt{2}}$  depends on the medium through which the neutrino propagates, and it arises due to matter effects encountered during neutrino propagation through the Earth. Here,  $G_F$  denotes the Fermi constant and  $N_e$  represents the electron number density of the medium. For Earth, the parameter  $a$  is approximately  $3500 \text{ km}^{-1}$  [39].

The CP asymmetry parameter  $A_{\mu e}$  can also be expressed in terms of physical parameters as:

$$A_{\mu e} = \frac{2\sqrt{P_{\text{atm}}} \sqrt{P_{\text{sol}}} \sin \Delta_{32} \sin \delta}{P_{\text{atm}} + 2\sqrt{P_{\text{atm}}} \sqrt{P_{\text{sol}}} \cos \Delta_{32} \cos \delta + P_{\text{sol}}}.$$

In this work, we analyze the CP asymmetry parameter in the context of three long-baseline neutrino experiments with different baseline lengths: T2K ( $L = 295$  km) [40], NO $\nu$ A ( $L = 810$  km) [41] and DUNE ( $L = 1300$  km) [42] (see Figs. 5(a)–5(c)). For this analysis, the neutrino beam energy  $E$  is varied within the range  $0.5 \text{ GeV} \leq E \leq 5 \text{ GeV}$ . We emphasize that the variation of the CP asymmetry parameter is examined based on the texture's predictions, by systematically considering different choices of baseline lengths and beam energies. The value of  $A_{\mu e}$  is significantly influenced by the Dirac CP phase,  $\delta$ . Long-baseline experiments aim to measure this phase while accounting for sub-dominant matter effects. Notably, the results from T2K ( $L = 295$  km) and NO $\nu$ A ( $L = 810$  km) show differing predictions for  $\delta$  under the inverted ordering [40, 41]. Future experiments such as DUNE ( $L = 1300$  km), with a peak beam energy of approximately  $2.5 \text{ GeV}$  [42], are expected to shed further light on this discrepancy, providing a potential test for our prediction of  $A_{\mu e}$ .

In the next section, we outline a symmetry framework that offers a possible origin for the proposed texture.

Fields	$D_{l_L}$	$(e_R, \mu_R, \tau_R)$	$(\nu_{e_R}, \nu_{\mu_R}, \nu_{\tau_R})$	$H$	$\Delta_1$	$\Delta_2$	$\xi$	$\eta$	$\chi$	$\psi$	$\kappa$
$SU(2)_L$	2	(1, 1, 1)	(1, 1, 1)	2	3	3	1	1	1	1	1
$U(1)_Y$	-1	(-2, -2, -2)	(0, 0, 0)	1	-2	2	0	0	0	0	0
$A_4$	3	(1, 1'', 1')	(1'', 1, 1')	3	3	3	1	1''	1	1'	1
$Z_{10}$	0	(0, 0, 0)	(0, 4, 8)	0	0	8	2	0	6	4	2
$Z_7$	-2	(4, 4, 4)	(6, 6, 6)	1	3	1	2	2	0	2	0

TABLE I. The transformation properties of various fields under  $SU(2)_L \otimes U(1)_Y \otimes A_4 \otimes Z_{10} \otimes Z_7$ .

## V. SYMMETRY PERSPECTIVE

In this section, we explore how the proposed texture (Eq. (1)) may be realized from first principles via a combination of one Type-I and two Type-II seesaw mechanisms [43]. For this, we extend the SM scalar sector by seven scalars and the group structure by a non-Abelian discrete symmetry group,  $A_4$  and two cyclic groups,  $Z_7$  and  $Z_{10}$ . The charge assignments of the fields under the extended group  $SU(2)_L \otimes U(1)_Y \otimes A_4 \otimes Z_{10} \otimes Z_7$  are given in Table I. The Yukawa Lagrangian under the said group is constructed in the following way,

$$\begin{aligned}
-\mathcal{L}_Y = & y_e(\bar{D}_{l_L} H) e_R + y_\mu(\bar{D}_{l_L} H) \mu_R + y_\tau(\bar{D}_{l_L} H) \tau_R + y_1(\bar{D}_{l_L} \tilde{H}) \nu_{e_R} + \frac{y_2}{\Lambda}(\bar{D}_{l_L} \tilde{H}) \nu_{\mu_R} \chi + \frac{y_3}{\Lambda}(\bar{D}_{l_L} \tilde{H}) \nu_{\tau_R} \kappa \\
& + \frac{y_c}{2}(\bar{\nu}_{e_R}^c \nu_{e_R}) \eta + \frac{y_a}{2}(\bar{\nu}_{\mu_R}^c \nu_{\mu_R}) \xi + \frac{y_b}{2}[(\bar{\nu}_{e_R}^c \nu_{\tau_R}) + (\bar{\nu}_{\tau_R}^c \nu_{e_R})] \xi + \frac{y_d}{2}(\bar{\nu}_{\tau_R}^c \nu_{\tau_R}) \psi + y_t(\bar{D}_{l_L} D_{l_L}^c) i \sigma_2 \tilde{\Delta}_1 \\
& + \frac{y_s}{\Lambda}(\bar{D}_{l_L} D_{l_L}^c) i \sigma_2 \tilde{\Delta}_2 \xi + h.c.,
\end{aligned} \tag{9}$$

where  $\Lambda$  is the cut-off scale of the theory. The auxiliary groups  $Z_7$  and  $Z_{10}$  are introduced to eliminate certain undesired terms that are allowed by  $A_4$ . The group  $Z_7$  is instrumental in forbidding Weinberg's dimension 5 operator,  $\frac{1}{\Lambda} \bar{D}_{l_L} \tilde{H} \tilde{H}^T D_{l_L}^c$  and other similar terms [44]. The product rules under the  $A_4$  group are given in Appendix A.

To obtain the proposed texture, the vacuum expectation values (vev) for the scalar fields are chosen as:  $\langle H \rangle_0 = (1, 0, 0)^T v_H$ ,  $\langle \Delta_1 \rangle_0 = (1, -1, -1)^T v_1$ ,  $\langle \Delta_2 \rangle_0 = (0, 1, -1)^T v_2$ ,  $\langle \xi \rangle_0 = v_\xi$ ,  $\langle \eta \rangle_0 = v_\eta$ ,  $\langle \chi \rangle_0 = v_\chi$ ,  $\langle \psi \rangle_0 = v_\psi$  and  $\langle \kappa \rangle_0 = v_\kappa$ . With this choice of the vev's, the charged lepton mass matrix is diagonal and the total Majorana neutrino mass matrix in our model can be schematically expressed as:

$$M = M^I + M^{II,1} + M^{II,2},$$

where  $M^I$  denotes the contribution from the Type-I seesaw, involving the scalar fields  $H$ ,  $\chi$ ,  $\xi$ ,  $\kappa$ ,  $\eta$  and  $\psi$ . The other two contributions,  $M^{II,1}$  and  $M^{II,2}$ , from the two Type-II seesaw's, originate from the fields,  $\Delta_1$ ,  $\Delta_2$  and  $\xi$ .

After the scalar fields acquire vev's,  $M$  becomes a function of the parameters:  $y_1, y_2, y_3, y_a, y_b, y_c, y_d, y_t, y_s, \Lambda, v_H, v_1, v_2, v_\chi, v_\xi, v_\kappa, v_\psi, v_\eta$  and  $M$  will reduce to  $M_\nu$  (Eq. (1)) with the following constraints,

$$\begin{aligned}
D_1 &= y_t v_1 = 3b, \\
D_2 &= \frac{y_s v_2 v_\xi}{\Lambda} = 3a, \\
D_3 &= \frac{y_d \Lambda^2 v_\psi}{v_H^2 v_\kappa^2 y_3^2} = \frac{2(2b - a + g + h)}{[4a^2 - 6ab - 3b^2 - 2bg + h^2 - 4a(g + h)]}, \\
D_4 &= \frac{y_a \Lambda^2 v_\xi}{v_H^2 v_\chi^2 y_2^2} = \frac{10}{5a - 10b + 9h}, \\
D_5 &= \frac{y_b \Lambda v_\xi}{v_H^2 v_\kappa y_1 y_3} = \frac{2(a - b - g)}{[4a^2 - 6ab - 3b^2 - 2bg + h^2 - 4a(g + h)]}, \\
D_6 &= \frac{y_c v_\psi}{v_H^2 v_\kappa^2 y_3^2} = \frac{2(3a + 2b + g - h)}{[4a^2 - 6ab - 3b^2 - 2bg + h^2 - 4a(g + h)]}.
\end{aligned} \tag{10}$$

It is to be mentioned that it is quite challenging to predict the Yukawa couplings individually. However, the present work visualizes the parameter space of the combinations of the model parameters  $D_i$ 's,  $i = 1, 2, \dots, 6$  as shown in Fig. 6.



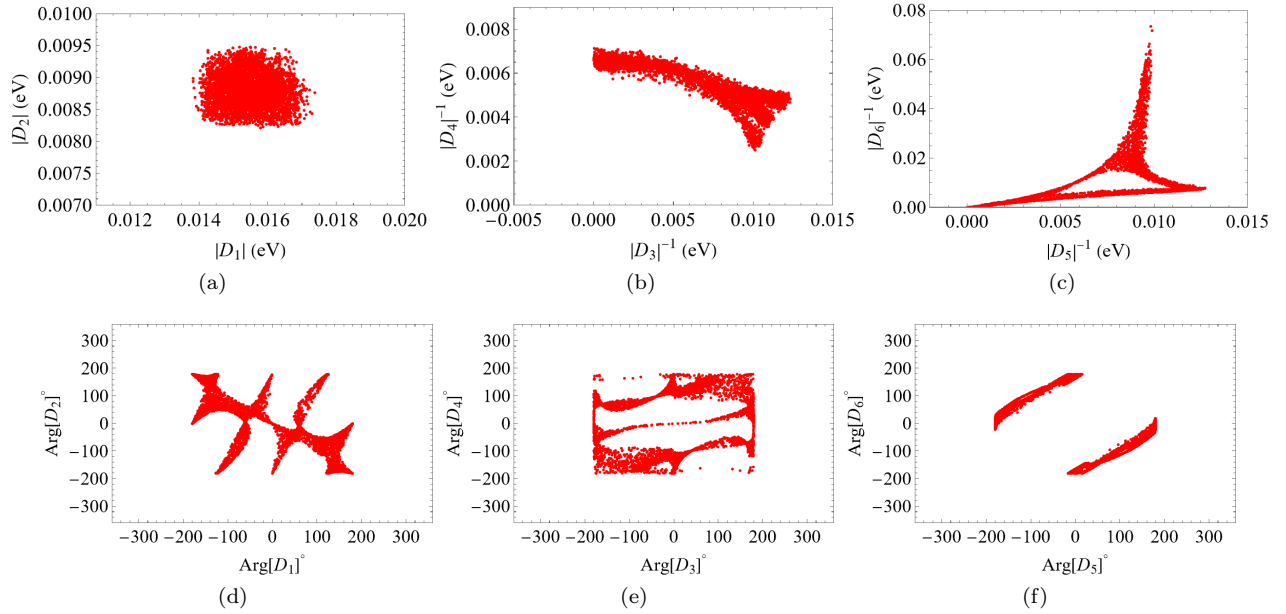


FIG. 6. The correlation plots between (a)  $|D_2|$  vs  $|D_1|$ , (b)  $|D_4|^{-1}$  vs  $|D_3|^{-1}$ , (c)  $|D_6|^{-1}$  vs  $|D_5|^{-1}$ , (d)  $\text{Arg}[D_2]$  vs  $\text{Arg}[D_1]$ , (e)  $\text{Arg}[D_4]$  vs  $\text{Arg}[D_3]$ , and (f)  $\text{Arg}[D_6]$  vs  $\text{Arg}[D_5]$  from model.

The  $SU(2)_L \otimes U(1)_Y \otimes A_4 \otimes Z_{10} \otimes Z_7$  invariant scalar potential along with the optimization conditions for the given choice of vev's is discussed in Appendix B. We now proceed to summarize the key findings of our work.

## VI. SUMMARY AND DISCUSSION

A new, minimal and predictive Majorana neutrino mass matrix texture is posited. Its various predictions are studied under a new mixing scheme: a partial TBM mixing where  $\sin \theta_{12} = 1/\sqrt{3}$  and  $\sin \theta_{23} = 1/\sqrt{2}$ , but  $\theta_{13}$  and  $\delta$  remain as free parameters. The texture rules out any possibility of  $\theta_{13}$  being zero and it is not a  $\mu - \tau$  deviated texture. We have seen that the observable parameters predicted by the texture depend on three real parameters, viz.,  $\text{Re}[h]$ ,  $\theta_{13}$  and  $\delta$ . We have randomized  $\theta_{13}$  and  $\delta$  within their  $3\sigma$  bounds and found two interesting cases emerge depending on the values of  $\text{Re}[h]$ . We have observed that when  $\text{Re}[h] > 0$ , some forbidden zones appear in the ranges for many observable parameters such as  $\theta_{13}$ ,  $\delta$ ,  $m_1$ ,  $m_2$ ,  $\Delta m_{21}^2$ ,  $\alpha$  and  $\beta$ . But such gaps drastically disappear when we consider the case,  $\text{Re}[h] < 0$ , with only  $\delta$  showing one. Notably, the Majorana phases are equal in both the cases.

We then extend our analysis beyond the partial TBM framework by randomizing  $\theta_{12}$  and  $\theta_{23}$  too in their  $3\sigma$  ranges and find that nor forbidden gaps are observed at all for any observable parameters. Interestingly, the Majorana phases are no longer equal. While the texture does not constrain the ranges of  $\theta_{12}$  and  $\theta_{13}$ , it predicts a narrow, symmetric range around  $45^\circ$  for  $\theta_{23}$ . The texture is found to favor only normal hierarchy for neutrino masses.

The texture may be realized from first principle with some reasonable constraints on model parameters. We have shown it under an extended symmetry group  $SU(2)_L \otimes U(1)_Y \otimes A_4 \otimes Z_{10} \otimes Z_7$  based on a hybrid framework of one Type-I seesaw and two Type-II seesaw mechanisms. The texture's phenomenological predictions make it a compelling framework for further investigation, particularly in the context of leptogenesis and its connection to the observed baryon asymmetry of the Universe.

## VII. ACKNOWLEDGEMENT

STG thanks Nihar Ranjan Saha, Indian Institute of Technology, Madras for a fruitful discussion on some aspects of numerical analysis. The research work of PC is supported by Innovation in Science Pursuit for Inspired Research (INSPIRE), Department of Science and Technology, Government of India, New Delhi vide grant No. IF190651.

### Appendix A: Product Rules of $A_4$

The non-Abelian discrete group,  $A_4$  has four inequivalent irreducible representations, viz., three singlets,  $1$ ,  $1'$  and  $1''$  and one triplet,  $3$ . In the Altarelli-Feruglio basis [15, 45], the multiplication rules take the following form:

$$\begin{aligned} \begin{pmatrix} a_1 \\ a_2 \\ a_3 \end{pmatrix}_3 \otimes \begin{pmatrix} b_1 \\ b_2 \\ b_3 \end{pmatrix}_3 &= (a_1 b_1 + a_2 b_3 + a_3 b_2)_1 \oplus (a_3 b_3 + a_1 b_2 + a_2 b_1)_{1'} \oplus (a_2 b_2 + a_1 b_3 + a_3 b_1)_{1''} \\ &\oplus \frac{1}{3} \begin{pmatrix} 2a_1 b_1 - a_2 b_3 - a_3 b_2 \\ 2a_3 b_3 - a_1 b_2 - a_2 b_1 \\ 2a_2 b_2 - a_1 b_3 - a_3 b_1 \end{pmatrix}_{3_s} \oplus \frac{1}{2} \begin{pmatrix} a_2 b_3 - a_3 b_2 \\ a_1 b_2 - a_2 b_1 \\ a_1 b_3 - a_3 b_1 \end{pmatrix}_{3_a}, \end{aligned}$$

and,

$$1 \otimes 1 = 1, \quad 1' \otimes 1'' = 1, \quad 1'' \otimes 1' = 1.$$

### Appendix B: The Scalar Potential

To justify the vacuum alignments of the scalar fields, we construct the  $SU(2)_L \otimes U(1)_Y \otimes A_4 \otimes Z_{10} \otimes Z_7$  invariant scalar potential as shown below,

$$\begin{aligned} V &= V(H) + V(\psi) + V(\eta) + V(\chi) + V(\kappa) + V(\xi) + V(\Delta_1) + V(\Delta_2) + V(H, \psi) + V(H, \eta) + V(H, \chi) \\ &\quad + V(H, \kappa) + V(H, \xi) + V(H, \Delta_1) + V(H, \Delta_2) + V(\psi, \eta) + V(\psi, \chi) + V(\psi, \kappa) + V(\psi, \xi) + V(\psi, \Delta_1) \\ &\quad + V(\psi, \Delta_2) + V(\eta, \chi) + V(\eta, \kappa) + V(\eta, \xi) + V(\eta, \Delta_1) + V(\eta, \Delta_2) + V(\chi, \kappa) + V(\chi, \xi) + V(\chi, \Delta_1) \\ &\quad + V(\chi, \Delta_2) + V(\kappa, \xi) + V(\kappa, \Delta_1) + V(\kappa, \Delta_2) + V(\xi, \Delta_1) + V(\xi, \Delta_2) + V(\Delta_1, \Delta_2) + h.c. \end{aligned}$$

The explicit forms of the terms appearing in the scalar potential are shown in the following,

$$\begin{aligned} V(H) &= -\mu_H^2 (H^\dagger H) + \lambda_1^H (H^\dagger H)(H^\dagger H) + \lambda_2^H (H^\dagger H)_{1'} (H^\dagger H)_{1''} + \lambda_3^H (H^\dagger H)_{3s} (H^\dagger H)_{3s} + \lambda_4^H (H^\dagger H)_{3s} \\ &\quad (H^\dagger H)_{3a} + \lambda_5^H (H^\dagger H)_{3a} (H^\dagger H)_{3a}, \\ V(\psi) &= -\mu_\psi^2 (\psi^\dagger \psi) + \lambda^\psi (\psi^\dagger \psi)(\psi^\dagger \psi), \\ V(\eta) &= -\mu_\eta^2 (\eta^\dagger \eta) + \lambda^\eta (\eta^\dagger \eta)(\eta^\dagger \eta), \\ V(\chi) &= -\mu_\chi^2 (\chi^\dagger \chi) + \lambda^\chi (\chi^\dagger \chi)(\chi^\dagger \chi), \\ V(\kappa) &= -\mu_\kappa^2 (\kappa^\dagger \kappa) + \lambda^\kappa (\kappa^\dagger \kappa)(\kappa^\dagger \kappa), \\ V(\xi) &= -\mu_\xi^2 (\xi^\dagger \xi) + \lambda^\xi (\xi^\dagger \xi)(\xi^\dagger \xi), \\ V(\Delta_1) &= -\mu_{\Delta_1}^2 \text{Tr}(\Delta_1^\dagger \Delta_1) + \lambda_1^{\Delta_1} \text{Tr}(\Delta_1^\dagger \Delta_1) \text{Tr}(\Delta_1^\dagger \Delta_1) + \lambda_2^{\Delta_1} \text{Tr}(\Delta_1^\dagger \Delta_1)_{1'} \text{Tr}(\Delta_1^\dagger \Delta_1)_{1''} + \lambda_3^{\Delta_1} \text{Tr}(\Delta_1^\dagger \Delta_1)_{3s} \\ &\quad \text{Tr}(\Delta_1^\dagger \Delta_1)_{3s} + \lambda_4^{\Delta_1} \text{Tr}(\Delta_1^\dagger \Delta_1)_{3s} \text{Tr}(\Delta_1^\dagger \Delta_1)_{3a} + \lambda_5^{\Delta_1} \text{Tr}(\Delta_1^\dagger \Delta_1)_{3a} \text{Tr}(\Delta_1^\dagger \Delta_1)_{3a}, \\ V(\Delta_2) &= -\mu_{\Delta_2}^2 \text{Tr}(\Delta_2^\dagger \Delta_2) + \lambda_1^{\Delta_2} \text{Tr}(\Delta_2^\dagger \Delta_2) \text{Tr}(\Delta_2^\dagger \Delta_2) + \lambda_2^{\Delta_2} \text{Tr}(\Delta_2^\dagger \Delta_2)_{1'} \text{Tr}(\Delta_2^\dagger \Delta_2)_{1''} + \lambda_3^{\Delta_2} \text{Tr}(\Delta_2^\dagger \Delta_2)_{3s} \\ &\quad \text{Tr}(\Delta_2^\dagger \Delta_2)_{3s} + \lambda_4^{\Delta_2} \text{Tr}(\Delta_2^\dagger \Delta_2)_{3s} \text{Tr}(\Delta_2^\dagger \Delta_2)_{3a} + \lambda_5^{\Delta_2} \text{Tr}(\Delta_2^\dagger \Delta_2)_{3a} \text{Tr}(\Delta_2^\dagger \Delta_2)_{3a}, \\ V(H, \psi) &= \lambda_1^{H\psi} (H^\dagger H)(\psi^\dagger \psi), \\ V(H, \eta) &= \lambda_1^{H\eta} (H^\dagger H)(\eta^\dagger \eta), \\ V(H, \chi) &= \lambda_1^{H\chi} (H^\dagger H)(\chi^\dagger \chi), \\ V(H, \kappa) &= \lambda_1^{H\kappa} (H^\dagger H)(\kappa^\dagger \kappa), \\ V(H, \xi) &= \lambda_1^{H\xi} (H^\dagger H)(\xi^\dagger \xi), \\ V(\psi, \eta) &= \lambda_1^{\psi\eta} (\psi^\dagger \psi)(\eta^\dagger \eta), \\ V(\psi, \chi) &= \lambda_1^{\psi\chi} (\psi^\dagger \psi)(\chi^\dagger \chi), \\ V(\psi, \kappa) &= \lambda_1^{\psi\kappa} (\psi^\dagger \psi)(\kappa^\dagger \kappa), \\ V(\psi, \xi) &= \lambda_1^{\psi\xi} (\psi^\dagger \psi)(\xi^\dagger \xi), \end{aligned}$$

$$\begin{aligned}
V(\psi, \Delta_1) &= \lambda_1^{\psi\Delta_1} \text{Tr}(\psi^\dagger \psi)(\Delta_1^\dagger \Delta_1), \\
V(\psi, \Delta_2) &= \lambda_1^{\psi\Delta_2} \text{Tr}(\psi^\dagger \psi)(\Delta_2^\dagger \Delta_2), \\
V(\eta, \chi) &= \lambda_1^{\eta\chi} (\eta^\dagger \eta)(\chi^\dagger \chi), \\
V(\eta, \kappa) &= \lambda_1^{\eta\kappa} (\eta^\dagger \eta)(\kappa^\dagger \kappa), \\
V(\eta, \xi) &= \lambda_1^{\eta\xi} (\eta^\dagger \eta)(\xi^\dagger \xi), \\
V(\eta, \Delta_1) &= \lambda_1^{\eta\Delta_1} \text{Tr}(\eta^\dagger \eta)(\Delta_1^\dagger \Delta_1), \\
V(\eta, \Delta_2) &= \lambda_1^{\eta\Delta_2} \text{Tr}(\eta^\dagger \eta)(\Delta_2^\dagger \Delta_2), \\
V(\chi, \kappa) &= \lambda_1^{\chi\kappa} (\chi^\dagger \chi)(\kappa^\dagger \kappa), \\
V(\chi, \xi) &= \lambda_1^{\chi\xi} (\chi^\dagger \chi)(\xi^\dagger \xi), \\
V(\chi, \Delta_1) &= \lambda_1^{\chi\Delta_1} \text{Tr}(\chi^\dagger \chi)(\Delta_1^\dagger \Delta_1), \\
V(\chi, \Delta_2) &= \lambda_1^{\chi\Delta_2} \text{Tr}(\chi^\dagger \chi)(\Delta_2^\dagger \Delta_2), \\
V(\kappa, \xi) &= \lambda_1^{\kappa\xi} (\kappa^\dagger \kappa)(\xi^\dagger \xi), \\
V(\kappa, \Delta_1) &= \lambda_1^{\kappa\Delta_1} \text{Tr}(\kappa^\dagger \kappa)(\Delta_1^\dagger \Delta_1), \\
V(\kappa, \Delta_2) &= \lambda_1^{\kappa\Delta_2} \text{Tr}(\kappa^\dagger \kappa)(\Delta_2^\dagger \Delta_2), \\
V(H, \Delta_1) &= \lambda_1^{H\Delta_1} (H^\dagger H) \text{Tr}(\Delta_1^\dagger \Delta_1) + \lambda_2^{H\Delta_1} \left[ (H^\dagger H)_{1'} \text{Tr}(\Delta_1^\dagger \Delta_1)_{1''} + (H^\dagger H)_{1''} \text{Tr}(\Delta_1^\dagger \Delta_1)_{1'} \right] + \lambda_3^{H\Delta_1} (H^\dagger H)_{3s} \\
&\quad \text{Tr}(\Delta_1^\dagger \Delta_1)_{3s} + \lambda_4^{H\Delta_1} \left[ (H^\dagger H)_{3s} \text{Tr}(\Delta_1^\dagger \Delta_1)_{3a} + (H^\dagger H)_{3a} \text{Tr}(\Delta_1^\dagger \Delta_1)_{3s} \right] + \lambda_5^{H\Delta_1} (H^\dagger H)_{3a} \text{Tr}(\Delta_1^\dagger \Delta_1)_{3a} \\
&\quad + Y_1 \eta (H^T i \sigma_2 \Delta_1^T H), \\
V(\xi, \Delta_1) &= \lambda_1^{\xi\Delta_1} \text{Tr}(\xi^\dagger \xi)(\Delta_1^\dagger \Delta_1), \\
V(H, \Delta_2) &= \lambda_1^{H\Delta_2} (H^\dagger H) \text{Tr}(\Delta_2^\dagger \Delta_2) + \lambda_2^{H\Delta_2} \left[ (H^\dagger H)_{1'} \text{Tr}(\Delta_2^\dagger \Delta_2)_{1''} + (H^\dagger H)_{1''} \text{Tr}(\Delta_2^\dagger \Delta_2)_{1'} \right] + \lambda_3^{H\Delta_2} (H^\dagger H)_{3s} \\
&\quad \text{Tr}(\Delta_2^\dagger \Delta_2)_{3s} + \lambda_4^{H\Delta_2} \left[ (H^\dagger H)_{3s} \text{Tr}(\Delta_2^\dagger \Delta_2)_{3a} + (H^\dagger H)_{3a} \text{Tr}(\Delta_2^\dagger \Delta_2)_{3s} \right] + \lambda_5^{H\Delta_2} (H^\dagger H)_{3a} \text{Tr}(\Delta_2^\dagger \Delta_2)_{3a} \\
&\quad + \frac{Y_2}{\Lambda} \psi \eta (H^T i \sigma_2 \Delta_2^T H), \\
V(\xi, \Delta_2) &= \lambda_1^{\xi\Delta_2} \text{Tr}(\xi^\dagger \xi)(\Delta_2^\dagger \Delta_2), \\
V(\Delta_1, \Delta_2) &= \lambda_1^{\Delta_1\Delta_2} \text{Tr}(\Delta_1^\dagger \Delta_1)(\Delta_2^\dagger \Delta_2),
\end{aligned}$$

Now for the VEV alignments of our choice, the following optimization conditions should be valid,

$$\begin{aligned}
&\frac{1}{36\Lambda} (v_H(15\sqrt{2} v_2 v_\eta v_\xi Y_2) + 8v_2^2 \Lambda(-9\lambda_1^{H\Delta_2} + 2\lambda_3^{H\Delta_2}) + 2\Lambda(-15v_1 v_\eta Y_1 + 54v_1^2 \lambda_1^{H\Delta_1} + 4v_H^2(9\lambda_1^H + 4\lambda_3^H) \\
&\quad + 18(v_\eta^2 \lambda_1^{H\eta} + v_\kappa^2 \lambda_1^{H\kappa} + v_\xi^2 \lambda_1^{H\xi} + v_\chi^2 \lambda_1^{H\chi} + v_\psi^2 \lambda_1^{H\psi} - 2\mu_H^2))) = 0, \\
&-\frac{1}{36} v_H(15v_1 v_\eta Y_1 + 4v_1^2(9\lambda_2^{H\Delta_1} + 4\lambda_3^{H\Delta_1}) + 4v_2^2(-9\lambda_2^{H\Delta_2} + 2\lambda_3^{H\Delta_2})) = 0, \\
&\frac{1}{72\Lambda} v_H(15\sqrt{2} v_2 v_\eta v_\xi Y_2 + 30v_1 v_\eta Y_1 \Lambda - 8v_1^2 \Lambda(9\lambda_2^{H\Delta_1} + 4\lambda_3^{H\Delta_1}) + 8v_2^2 \Lambda(9\lambda_2^{H\Delta_2} - 2\lambda_3^{H\Delta_2})) \\
&= 0, \\
&v_1(v_\eta^2 \lambda_1^{\Delta_1\eta} + v_\kappa^2 \lambda_1^{\Delta_1\kappa} + v_\xi^2 \lambda_1^{\Delta_1\xi} + v_\chi^2 \lambda_1^{\Delta_1\chi} + v_\psi^2 \lambda_1^{\Delta_1\psi} + v_H^2(\lambda_1^{H\Delta_1} + \frac{4}{9}\lambda_3^{H\Delta_1}) + v_1^2(6\lambda_1^{\Delta_1} + 2\lambda_2^{\Delta_1} + \frac{16}{9}\lambda_3^{\Delta_1}) \\
&\quad - 2\mu_{\Delta_1}^2) = 0, \\
&v_H^2(\frac{5}{12}v_\eta Y_1 - v_1 \lambda_1^{H\Delta_1} + \frac{2}{9}v_1 \lambda_3^{H\Delta_1}) - \frac{2}{3}v_1^3(9\lambda_1^{\Delta_1} + 4\lambda_3^{\Delta_1}) - v_1(v_\eta^2 \lambda_1^{\Delta_1\eta} + v_\kappa^2 \lambda_1^{\Delta_1\kappa} + v_\xi^2 \lambda_1^{\Delta_1\xi} + v_\chi^2 \lambda_1^{\Delta_1\chi} + v_\psi^2 \lambda_1^{\Delta_1\psi} \\
&\quad - 2\mu_{\Delta_1}^2) = 0, \\
&\frac{1}{9}v_1(v_H^2(9\lambda_1^{H\Delta_1} - 2\lambda_3^{H\Delta_1}) + 6v_1^2(9\lambda_1^{\Delta_1} + 4\lambda_3^{\Delta_1}) + 9(v_\eta^2 \lambda_1^{\Delta_1\eta} + v_\kappa^2 \lambda_1^{\Delta_1\kappa} + v_\xi^2 \lambda_1^{\Delta_1\xi} + v_\chi^2 \lambda_1^{\Delta_1\chi} + v_\psi^2 \lambda_1^{\Delta_1\psi} - 2\mu_{\Delta_1}^2)) \\
&= 0,
\end{aligned}$$

$$\begin{aligned}
& v_H^2 \left( \frac{5}{12\sqrt{2}\Lambda} v_\eta v_\xi Y_2 - v_2 \lambda_1^{H\Delta_2} + \frac{2}{9} v_2 \lambda_3^{H\Delta_2} \right) + v_2^3 (4\lambda_1^{\Delta_2} + \lambda_2^{\Delta_2} + \frac{4}{3} \lambda_3^{\Delta_2}) - v_2 (v_\eta^2 \lambda_1^{\Delta_2\eta} + v_\kappa^2 \lambda_1^{\Delta_2\kappa} + v_\xi^2 \lambda_1^{\Delta_2\xi} + v_\chi^2 \\
& \lambda_1^{\Delta_2\chi} + v_\psi^2 \lambda_1^{\Delta_2\psi} - 2\mu_{\Delta_2}^2) = 0, \\
& v_H^2 v_2 (\lambda_1^{H\Delta_2} - \frac{2}{9} \lambda_3^{H\Delta_2}) - \frac{1}{3} v_2^3 (12\lambda_1^{\Delta_2} + 3\lambda_2^{\Delta_2} + 4\lambda_3^{\Delta_2}) + v_2 (v_\eta^2 \lambda_1^{\Delta_2\eta} + v_\kappa^2 \lambda_1^{\Delta_2\kappa} + v_\xi^2 \lambda_1^{\Delta_2\xi} + v_\chi^2 \lambda_1^{\Delta_2\chi} + v_\psi^2 \lambda_1^{\Delta_2\psi} \\
& - 2\mu_{\Delta_2}^2) = 0, \\
& v_H^2 \left( -\frac{5}{12} v_1 Y_1 + \frac{5}{12\sqrt{2}\Lambda} v_2 v_\xi Y_2 + v_\eta \lambda_1^{H\eta} \right) + v_\eta (3v_1^2 \lambda_1^{\Delta_1\eta} + v_\kappa^2 \lambda_1^{\eta\kappa} + v_\xi^2 \lambda_1^{\xi\eta} - 2v_2^2 \lambda_1^{\Delta_2\eta} + v_\chi^2 \lambda_1^{\chi\eta} + v_\psi^2 \lambda_1^{\psi\eta} + 2v_\eta^2 \\
& \lambda^\eta - 2\mu_\eta^2) = 0, \\
& v_\kappa (v_H^2 \lambda_1^{H\kappa} + 3v_1^2 \lambda_1^{\Delta_1\kappa} + v_\eta^2 \lambda_1^{\eta\kappa} + v_\xi^2 \lambda_1^{\xi\kappa} - 2v_2^2 \lambda_1^{\Delta_2\kappa} + v_\chi^2 \lambda_1^{\chi\kappa} + v_\psi^2 \lambda_1^{\psi\kappa} + 2v_\kappa^2 \lambda^\kappa - 2\mu_\kappa^2) = 0, \\
& v_H^2 \left( \frac{5}{12\sqrt{2}\Lambda} v_2 v_\eta Y_2 + v_\xi \lambda_1^{H\xi} \right) + v_\xi (3v_1^2 \lambda_1^{\Delta_1\xi} + v_\eta^2 \lambda_1^{\xi\eta} + v_\kappa^2 \lambda_1^{\xi\kappa} - 2v_2^2 \lambda_1^{\Delta_2\xi} + v_\chi^2 \lambda_1^{\chi\xi} + v_\psi^2 \lambda_1^{\psi\xi} + 2v_\xi^2 \lambda^\xi - 2\mu_\xi^2) = 0, \\
& v_\psi (v_H^2 \lambda_1^{H\psi} + 3v_1^2 \lambda_1^{\Delta_1\psi} - 2v_2^2 \lambda_1^{\Delta_2\psi} + v_\chi^2 \lambda_1^{\chi\psi} + v_\eta^2 \lambda_1^{\psi\eta} + v_\kappa^2 \lambda_1^{\psi\kappa} + v_\xi^2 \lambda_1^{\psi\xi} + 2v_\psi^2 \lambda^\psi - 2\mu_\psi^2) = 0, \\
& v_\chi (v_H^2 \lambda_1^{H\chi} + 3v_1^2 \lambda_1^{\Delta_1\chi} - 2v_2^2 \lambda_1^{\Delta_2\chi} + v_\eta^2 \lambda_1^{\chi\eta} + v_\kappa^2 \lambda_1^{\chi\kappa} + v_\xi^2 \lambda_1^{\chi\xi} + v_\psi^2 \lambda_1^{\chi\psi} + 2v_\chi^2 \lambda^\chi - 2\mu_\chi^2) = 0. \tag{B1}
\end{aligned}$$

In the context of scalar potentials and minimization conditions, the analysis strategy is nontrivial. The present framework involves eight scalar field triplets  $H, \Delta_1, \Delta_2, \chi, \xi, \kappa, \psi$  and  $\eta$ , which together contribute 55 real scalar degrees of freedom. This results in 55 independent extremization (minimization) conditions, out of which the nontrivial ones are listed in Eq. (B1). To verify whether a chosen vacuum alignment corresponds to a true minimum, one must evaluate the Hessian matrix:  $\left. \frac{\partial^2 V}{\partial \phi_i \partial \phi_j} \right|_0$ , where  $V$  denotes the scalar potential, and the second derivatives are evaluated at the vev's. A necessary condition for the vacuum to represent a local minimum is that all eigenvalues of the Hessian be positive (with zero eigenvalues allowed in Goldstone directions). Equivalently, this is ensured if all principal minors of the Hessian are positive, indicating that the matrix is positive definite. In our case, the Hessian is a  $55 \times 55$  matrix, making a complete eigenvalue analysis computationally demanding. Instead, we adopt a practical approach by analyzing the structure of the optimization conditions, which depend on 74 free parameters: eight  $\mu^2$  type mass terms, 58 quartic couplings  $\lambda$ 's and eight vev's. By tuning these parameters appropriately, one can satisfy the required conditions for vacuum stability. However, a full exploration of the potential landscape is beyond the scope of the present work.

- 
- [1] R. Davis, Jr., D. S. Harmer, and K. C. Hoffman, Search for neutrinos from the sun, Phys. Rev. Lett. **20**, 1205 (1968).
  - [2] Q. R. Ahmad *et al.* (SNO), Measurement of the rate of  $\nu_e + d \rightarrow p + p + e^-$  interactions produced by  $^8\text{B}$  solar neutrinos at the Sudbury Neutrino Observatory, Phys. Rev. Lett. **87**, 071301 (2001), arXiv:nucl-ex/0106015.
  - [3] S. Fukuda *et al.* (Super-Kamiokande), Solar B-8 and hep neutrino measurements from 1258 days of Super-Kamiokande data, Phys. Rev. Lett. **86**, 5651 (2001), arXiv:hep-ex/0103032.
  - [4] R. M. Bionta *et al.*, Observation of a Neutrino Burst in Coincidence with Supernova SN 1987a in the Large Magellanic Cloud, Phys. Rev. Lett. **58**, 1494 (1987).
  - [5] Y. Fukuda *et al.* (Super-Kamiokande), Evidence for oscillation of atmospheric neutrinos, Phys. Rev. Lett. **81**, 1562 (1998), arXiv:hep-ex/9807003.
  - [6] K. Eguchi *et al.* (KamLAND), First results from KamLAND: Evidence for reactor anti-neutrino disappearance, Phys. Rev. Lett. **90**, 021802 (2003), arXiv:hep-ex/0212021.
  - [7] F. P. An *et al.* (Daya Bay), Observation of electron-antineutrino disappearance at Daya Bay, Phys. Rev. Lett. **108**, 171803 (2012), arXiv:1203.1669 [hep-ex].
  - [8] M. H. Ahn *et al.* (K2K), Indications of neutrino oscillation in a 250 km long baseline experiment, Phys. Rev. Lett. **90**, 041801 (2003), arXiv:hep-ex/0212007.
  - [9] K. Abe *et al.* (T2K), Observation of Electron Neutrino Appearance in a Muon Neutrino Beam, Phys. Rev. Lett. **112**, 061802 (2014), arXiv:1311.4750 [hep-ex].
  - [10] K. S. Hirata *et al.* (Kamiokande-II), Observation of B-8 Solar Neutrinos in the Kamiokande-II Detector, Phys. Rev. Lett. **63**, 16 (1989).
  - [11] I. Esteban, M. C. Gonzalez-Garcia, M. Maltoni, I. Martinez-Soler, J. a. P. Pinheiro, and T. Schwetz, NuFit-6.0: updated global analysis of three-flavor neutrino oscillations, JHEP **12**, 216, arXiv:2410.05380 [hep-ph].
  - [12] R. L. Workman *et al.* (Particle Data Group), Review of Particle Physics, PTEP **2022**, 083C01 (2022).
  - [13] S. F. King and C. C. Nishi, Mu-tau symmetry and the Littlest Seesaw, Phys. Lett. B **785**, 391 (2018), arXiv:1807.00023 [hep-ph].

- [14] Z.-z. Xing and Z.-h. Zhao, A review of  $\mu$ - $\tau$  flavor symmetry in neutrino physics, Rept. Prog. Phys. **79**, 076201 (2016), arXiv:1512.04207 [hep-ph].
- [15] G. Altarelli and F. Feruglio, Tri-bimaximal neutrino mixing, A(4) and the modular symmetry, Nucl. Phys. B **741**, 215 (2006), arXiv:hep-ph/0512103.
- [16] P. O. Ludl and W. Grimus, A complete survey of texture zeros in the lepton mass matrices, JHEP **07**, 090, [Erratum: JHEP **10**, 126 (2014)], arXiv:1406.3546 [hep-ph].
- [17] R. Kalita and D. Borah, Hybrid Textures of Neutrino Mass Matrix under the Lamppost of Latest Neutrino and Cosmology Data, Int. J. Mod. Phys. A **31**, 1650008 (2016), arXiv:1509.02728 [hep-ph].
- [18] M. Singh, Investigating the hybrid textures of neutrino mass matrix for near maximal atmospheric neutrino mixing, Adv. High Energy Phys. **2018**, 5806743 (2018), arXiv:1803.10754 [hep-ph].
- [19] P. F. Harrison, D. H. Perkins, and W. G. Scott, Tri-bimaximal mixing and the neutrino oscillation data, Phys. Lett. B **530**, 167 (2002), arXiv:hep-ph/0202074.
- [20] S. F. King, Constructing the large mixing angle MNS matrix in seesaw models with right-handed neutrino dominance, JHEP **09**, 011, arXiv:hep-ph/0204360.
- [21] P. H. Frampton, S. T. Petcov, and W. Rodejohann, On deviations from bimaximal neutrino mixing, Nucl. Phys. B **687**, 31 (2004), arXiv:hep-ph/0401206.
- [22] G. Altarelli, F. Feruglio, and I. Masina, Can neutrino mixings arise from the charged lepton sector?, Nucl. Phys. B **689**, 157 (2004), arXiv:hep-ph/0402155.
- [23] J. Ganguly, J. Gluza, and B. Karmakar, Common origin of  $\theta_{13}$  and dark matter within the flavor symmetric scoto-seesaw framework, JHEP **11**, 074, arXiv:2209.08610 [hep-ph].
- [24] D. Borah, B. Karmakar, and D. Nanda, Planck scale origin of nonzero  $\theta_{13}$  and super-WIMP dark matter, Phys. Rev. D **100**, 055014 (2019), arXiv:1906.02756 [hep-ph].
- [25] W. Rodejohann, Type II seesaw mechanism, deviations from bimaximal neutrino mixing and leptogenesis, Phys. Rev. D **70**, 073010 (2004), arXiv:hep-ph/0403236.
- [26] D. Borah, Deviations from Tri-Bimaximal Neutrino Mixing Using Type II Seesaw, Nucl. Phys. B **876**, 575 (2013), arXiv:1307.2426 [hep-ph].
- [27] S. F. King and C. Luhn, Trimaximal neutrino mixing from vacuum alignment in A4 and S4 models, JHEP **09**, 042, arXiv:1107.5332 [hep-ph].
- [28] M. Honda and M. Tanimoto, Deviation from tri-bimaximal neutrino mixing in A(4) flavor symmetry, Prog. Theor. Phys. **119**, 583 (2008), arXiv:0801.0181 [hep-ph].
- [29] Z. Maki, M. Nakagawa, and S. Sakata, Remarks on the unified model of elementary particles, Prog. Theor. Phys. **28**, 870 (1962).
- [30] N. Aghanim *et al.* (Planck), Planck 2018 results. VI. Cosmological parameters, Astron. Astrophys. **641**, A6 (2020), [Erratum: Astron.Astrophys. 652, C4 (2021)], arXiv:1807.06209 [astro-ph.CO].
- [31] J. Schechter and J. W. F. Valle, Neutrinoless Double beta Decay in SU(2) x U(1) Theories, Phys. Rev. D **25**, 2951 (1982).
- [32] H. Ejiri, Neutrino-Mass Sensitivity and Nuclear Matrix Element for Neutrinoless Double Beta Decay, Universe **6**, 225 (2020).
- [33] M. Agostini, G. Benato, J. A. Detwiler, J. Menéndez, and F. Vissani, Toward the discovery of matter creation with neutrinoless  $\beta\beta$  decay, Rev. Mod. Phys. **95**, 025002 (2023), arXiv:2202.01787 [hep-ex].
- [34] D. Q. Adams *et al.* (CUORE), Improved Limit on Neutrinoless Double-Beta Decay in  $^{130}\text{Te}$  with CUORE, Phys. Rev. Lett. **124**, 122501 (2020), arXiv:1912.10966 [nucl-ex].
- [35] M. Agostini *et al.* (GERDA), Probing Majorana neutrinos with double- $\beta$  decay, Science **365**, 1445 (2019), arXiv:1909.02726 [hep-ex].
- [36] A. Gando *et al.* (KamLAND-Zen), Search for Majorana Neutrinos near the Inverted Mass Hierarchy Region with KamLAND-Zen, Phys. Rev. Lett. **117**, 082503 (2016), [Addendum: Phys.Rev.Lett. 117, 109903 (2016)], arXiv:1605.02889 [hep-ex].
- [37] R. Arnold *et al.* (SuperNEMO), Measurement of the distribution of  $^{207}\text{Bi}$  depositions on calibration sources for SuperNEMO, JINST **16** (07), T07012, arXiv:2103.14429 [physics.ins-det].
- [38] N. Abgrall *et al.* (LEGEND), The Large Enriched Germanium Experiment for Neutrinoless  $\beta\beta$  Decay: LEGEND-1000 Preconceptual Design Report, (2021), arXiv:2107.11462 [physics.ins-det].
- [39] R. Sinha, P. Roy, and A. Ghosal, CP transformed mixed  $\mu\tau$  antisymmetry for neutrinos and its consequences, Phys. Rev. D **99**, 033009 (2019), arXiv:1809.06615 [hep-ph].
- [40] K. Abe *et al.* (T2K), Constraint on the matter-antimatter symmetry-violating phase in neutrino oscillations, Nature **580**, 339 (2020), [Erratum: Nature 583, E16 (2020)], arXiv:1910.03887 [hep-ex].
- [41] M. A. Acero *et al.* (NOvA), Improved measurement of neutrino oscillation parameters by the NOvA experiment, Phys. Rev. D **106**, 032004 (2022), arXiv:2108.08219 [hep-ex].
- [42] B. Abi *et al.* (DUNE), Deep Underground Neutrino Experiment (DUNE), Far Detector Technical Design Report, Volume II: DUNE Physics, (2020), arXiv:2002.03005 [hep-ex].
- [43] P. Chakraborty, M. Dey, B. Karmakar, and S. Roy, Neutrino mixing from a fresh perspective, Phys. Lett. B **858**, 139020 (2024), arXiv:2405.10353 [hep-ph].
- [44] V. V. Vien, Neutrino mass and mixing from a novel scenario with  $A_4$  symmetry, Eur. Phys. J. Plus **140**, 399 (2025).
- [45] H. Ishimori, T. Kobayashi, H. Ohki, Y. Shimizu, H. Okada, and M. Tanimoto, Non-Abelian Discrete Symmetries in Particle Physics, Prog. Theor. Phys. Suppl. **183**, 1 (2010), arXiv:1003.3552 [hep-th].